

Mode decomposition evolution equations

Yang Wang¹, Guo Wei Wei^{1,2} and Siyang Yang¹

¹Department of Mathematics

Michigan State University, MI 48824, USA

²Department of Electrical and Computer Engineering

Michigan State University, MI 48824, USA

December 30, 2010

Abstract

Noise removal, image edge detection, distortion restoration, enhancement, segmentation, and pattern recognition are fundamental to signal processing, image processing, computer vision, machine vision, artificial intelligence and have applications to automatic control, robotics, sonar, radar, remote sensing, target tracking, communication, navigation and a variety of imaging technologies. Partial differential equation (PDE) based methods have become some of the most powerful tools for these problems in the past two decades. The advantages of PDE based approaches are that they can be made fully automatic, robust for the analysis of images, videos and high dimensional data. A fundamental question is whether one can use PDEs to perform all the basic tasks in the image processing. To certain extent, this is equivalent to asking whether one can devise PDEs to perform a full-scale mode decomposition for signals and images because when all the mode components are available, it is trivial to manipulate them for all image processing purposes. Despite of great progress in PDE based image analysis in the past two decades, the basic roles of PDEs in image/signal analysis are only limited to PDE based low-pass filters, and their applications to noise removal, edge detection, segmentation, etc. At present, it is not clear how to construct PDE based methods for full-scale mode decomposition. The above-mentioned limitation of most current PDE based image/signal processing methods is addressed in the proposed work, in which we introduce a family of mode decomposition evolution equations (MoDEEs) for a vast variety of applications. MoDEEs are inspired by the iterative filtering decomposition (IFD) (*Adv. Adapt. Data Analysis.*, 1(4): 543, 2009) and constructed as an extension of a PDE based high-pass filter (*Europhys. Lett.*, 59(6): 814, 2002) by using arbitrarily high order PDE based low-pass filters introduced by Wei (*IEEE Signal Process. Lett.*, 6(7): 165, 1999). Similar to the Fourier transform and wavelet transform, the present MoDEEs allow a perfect reconstruction of the original function. However, modes generated from the present approach are in the spatial or time domain and can be easily used for secondary processing. Various simplifications of the proposed MoDEEs, including a linearized version, and an algebraic version, are discussed for computational convenience. The Fourier pseudospectral method, which is unconditionally stable for linearized high order MoDEEs, is utilized in our computation. Validation is carried out to mode separation of high frequency adjacent modes. Applications are considered to signal and image denoising, image edge detection, feature extraction, enhancement etc. It is hoped that this work enhances the understanding of high-order PDEs and yields robust and useful tools for image and signal analysis.

Key words: Mode decomposition; Evolution equations; High order PDE transform; Anisotropic diffusion; Total variation; High-pass filter; Partial differential equation.

Contents

I	Introduction	3
II	Theory and formulation	6
II.A	High order PDE based low-pass filters	6
II.B	Nonlinear PDE based high-pass filters	6
II.C	Mode decomposition evolution equations (MoDEEs)	7
III	Simplified models and computational algorithms	8
III.A	Linear MoDEEs	8
III.B	Algebraic MoDEEs	9
III.C	Numerical methods for high-order MoDEEs	10
IV	Numerical tests and validations	10
IV.A	Intrinsic mode decomposition	10
IV.B	Image denoising, edge detection and enhancement	12
V	Applications	18
V.A	Magnetic resonance images	18
V.B	Magnetic resonance angiography images	19
V.C	X-ray computed tomography images	20
VI	Concluding remarks	21

I Introduction

Noise removal, image edge detection, distortion restoration, feature extraction, enhancement, segmentation and pattern recognition are fundamental problems in signal processing, image processing, computer vision, machine vision and artificial intelligence.^{15,21,62} The understanding of these problems and the construction of efficient solutions are essential to optical sorting, automatic control, augmented reality, robotics, sonar, radar, remote sensing, target tracking, surveillance, communication, navigation and a variety of imaging technologies. The primary step toward a solution to these problems is the decomposition of the original signal – image or general data – into various modes according to their frequency distributions. Usually, the subsequent analysis or secondary processing on individual mode components enables us to achieve our goal of processing. Therefore, mode decomposition is a fundamental process in information processing and data analysis.

Fourier analysis^{15,40,52,63,69} is one of the oldest techniques and remains one of the most useful techniques for mode decomposition. However, Fourier analysis is subject to a number of limitations. For example, Fourier method is not suitable for analyzing data of non-stationary nature. Moreover, Fourier analysis is not data adaptive. In many applications in signal processing, one usually desires information of spatial and temporal localization, which is also lack in Fourier analysis because of its global nature. Most importantly, when the signal or image involves abundantly many modes, the subsequent analysis or secondary processing becomes awkward if it is not fully automatic.

Wavelet transform is another powerful tool for mode decomposition.^{15,19,21,35,44,50,62,74} Similar to the Fourier analysis, wavelet transform decomposes a signal or image into frequency sub-bands which correspond to different temporal/spatial scales or resolutions. In this sense, wavelets are often used as filter banks.⁴⁴ Because the number of sub-bands is usually significantly smaller than that of the Fourier modes, it is much more convenient to carry out the secondary processing on individual sub-band than on individual Fourier mode. Additionally, via appropriate selection of wavelet functions and parameters, wavelet transform is able to provide controlled time-frequency or spatial-temporal localization. Moreover, wavelet analysis can be made fully adaptive and automatic for time varying and non-stationary signal and data. For these reasons, wavelet analysis has become very popular in many applied fields. However, wavelet transform is basically a linear analysis and suffers from many limitations. The down sides include uniformly poor frequency resolution, and sometimes counter-intuitive interpretation.³¹ In fact, wavelet methods inherit many shortcomings of the Fourier transform since some commonly used wavelets are based on Fourier analysis.

In approximation theory, mode decomposition can be achieved by the projection onto an orthogonal basis normalized in an appropriate norm. The aforementioned Fourier transform can be seen as a form of polynomial projection with harmonic base functions, i.e., trigonometric polynomials. Wavelet bases are usually constructed by a variety of means, such as spline functions and rational functions, in addition to many others. The technique of rational functions is a generalization based on the ratios of polynomial functions. In the Hilbert space analysis, a wide variety of polynomials can be used to construct suitable L^2 bases, depending on the geometric property of polynomials. The most commonly used polynomial functions include Chebyshev, Hermite, Legendre and Lagrange.⁴⁴ Many classical bases are unified in the sense of the Sturm-Liouville theory. In fact, for a well-defined weight function and appropriate geometric domain, one can construct a polynomial basis which is orthogonal with respect to the given weight.

More recently, empirical mode decomposition (EMD)^{17,31,33,57,67} has been constructed. Unlike the previous orthogonal decomposition methods, EMD aims to decompose signals and images of arbitrary dimensionality into multiple general hierarchical modes, based on which a secondary processing can be performed. Wang and his coworkers introduced iterative filtering decomposition (IFD).^{41,45,47} EMD and IFD modes are hierarchical in a sense that they are not orthogonal to each other, although there is a perfect reconstruction of the original signal and image from these modes. These modes are called intrinsic mode functions (IMFs).^{31,33,70} Time series or signals are decomposed into a sum of IMFs which have zero mean value and equal (or different by one) number of extrema and zero crossings. Each IMF contains information of instantaneous frequency defined by Hilbert-Huang transforms.^{20,32}

Additionally, EMD and IFD are highly data adaptive and applicable to non-uniform and non-stationary data.^{31,33,38,42,56,66}

Mode decomposition enables one to collect, filter and extract detailed information and knowledge corresponding to various individual modes. These modes could contain information related to frequency distribution, noise distribution, feature allotting, morphology, dynamics and transport of non-stationary signals, and images functions. Apart from applications to signal/image processing, data analysis, remote sensing, target tracking, and surveillance, mode decomposition methods can also be applied to many other fields, such as regression analysis,⁸⁵ linear programming, machine learning,^{46,48} and the solution of partial differential equations.⁷⁵ Each of these subjects has its own mathematical foundation and fruitful applications in science and engineering. However, a detailed elaboration of these aspects is beyond the scope of the present work.

An elementary operation of signal and image processing is filtering, i.e., the preservation of certain mode components and the elimination of others. Commonly used filters include low-pass, high-pass, band-pass, band-stop and all-pass ones. Among them, low-pass filters are widely used for denoising, whereas high-pass filters are commonly used for image edge detection. A vast variety of filters, such as linear, nonlinear, active, passive, wavelet, Chebyshev, Gaussian, Kalman, Wiener and conjugate filters,^{27,64,65} have been constructed for various applications. The essence that underpins the filtering process is the ability and efficiency of performing mode decomposition or frequency separation. In fact, one can do a lot more than filtering if all mode components are available. For example, one can perform secondary processing on each of the mode components before assembling them into desirable objects. One can also classify individual modes into certain categories, such as noise, image edge, image segment and smooth image before carrying out the secondary processing.

Witkin introduced the diffusion equation for image denoising in 1983.⁷⁹ The essential idea behind Witkin's method is that the evolution of an image under a diffusion operator is formally equivalent to the standard Gaussian low-pass filter. Consequently, image denoising can be formulated as an initial value problem of the diffusion equation. The solution to this partial differential equation (PDE) at a later time is a modified smooth image. Nevertheless, the original diffusion equation was not very efficient in denoising — it not only removes the noise but also smears the image edges, which leads to poor visual perception. This problem was addressed by Perona and Malik with an anisotropic diffusion equation,⁵³ in which the constant diffusion coefficient is replaced by a function of image gradients. The essential idea is to make the diffusion coefficient small at the image edges which contribute to large gradients. It was commonly believed that the nonlinear anisotropic diffusion equation facilitates a potentially more effective PDE algorithm for noise removing, image restoration, edge detection, and image enhancement. However, it was shown by further studies that the anisotropic diffusion operator may break down when the gradient generated by noise is comparable to image edges and features.^{11,51} One can of course apply a pre-convolution with a smoothing function to the image to reduce grey scale oscillation and to alleviate the instability, but the image quality will inevitably be degraded. One alternative solution introduced by Wei⁷³ is to statistically discriminate noise from image edges by a measure based on the local statistical variance of the image. Such a local statistical variance based edge-stopping works well for image restoration. PDE based methods have attracted great attention in the past two decades.^{4,6,10,14,26,34,37,54,60,80}

Rudin, Osher and Fatemi⁵⁸ devised image processing as a total variation (TV) problem. The essential idea is that signals and images with extra and possibly spurious components have a relatively large variation or gradient. As such, image processing can be formulated as a problem of minimizing the total energy defined as a functional of the gradient of the image, while preserving important image contents such as edges. The goal of the total energy variation is to reconstruct an image with the best fidelity and the least noise. However, this inverse problem is ill-posed in sense of Hadamard. Regularization procedures are usually used in total variation analysis. The use of different norm measurements for the fidelity term can affect the quality of image restoration. For example, L^2 norm based least square algorithms may produce smooth restoration which is inaccurate if the image consists of detailed features such as edges. In contrast, L^1 norm algorithms better preserve the edge information in the restored

images. The minimization is carried out with the calculus of variations which gives the minimum of the energy functional as the solution of the Euler-Lagrange equation.^{1,14} The TV concept provides a rigorous mathematical algorithm to introduce nonlinear diffusion equations and has been employed as a regularization approach for many applications where one needs to preserve discontinuous features.¹²

To improve the efficiency of noise removing, fourth-order evolution equations were introduced in the literature for image denoising and restoration.^{13,24,43,68,73,83} These equations were proposed either as a high-order generalization of the Perona-Malik equation⁷³ or as an extension of the TV formulation.^{13,43,68,83} Among these approaches, the generalized Perona-Malik equations introduced by Wei in 1999 were of arbitrarily high order.⁷³ The essential assumption in these high order equations is that high-order diffusion operators are able to remove high frequency components more efficiently. Mathematical analysis of these high order equations in Sobolev space was carried out by Bertozzi and Greer,^{7,24,25} which proved the existence and uniqueness of the solution to a case with H^1 initial data and a regularized operator. Similar analysis was performed by Xu and Zhou.⁸¹ Jin and Yang proved the existence of strong solution of the fourth-order generalized Perona-Malik equation.³⁶ Witelski and Bowen proposed alternating-direction implicit (ADI) schemes for high order image processing PDEs.⁷⁸

Image processing PDEs of the Perona-Malik type and total variation type are mostly designed to function as nonlinear low-pass filters. In 2002, Wei and Jia⁷⁶ introduced coupled nonlinear PDEs to behave as high-pass filters. These coupled PDEs are used for image edge detection. The essential idea behind these PDE based high-pass filters is that when two Perona-Malik type of PDEs evolve at dramatically different speeds, the difference of their solutions gives rise to image edges. This follows from the fact that the difference between an all-pass filter (i.e., identity operator) and a low-pass one is a high-pass filter.⁷⁶ The speeds of evolution in these equations are controlled by the appropriate selection of the diffusion coefficients. These PDE-based edge detectors have been shown to work extremely well for images with large amount of textures.^{64,76}

Despite of great progress in PDE based image analysis in the past two decades, a fundamental question is whether one can use PDEs to perform all tasks in the image processing. To certain extent, this is equivalent to ask whether one can devise PDEs to perform a full-scale mode decomposition for signals and images. As discussed earlier, when all the mode components are available, it is trivial to manipulate them for all image processing purposes. The main difficulty at present is that it is still unclear how to formulate PDEs for mode decomposition. The objective of the present work to construct a PDE based algorithm for mode decomposition of signals, images and functions. All of the important building blocks were developed in our earlier work, i.e., arbitrarily high order PDE filters⁷³ and PDE based high-pass filters.⁷⁶ The final construction of mode decomposition evolution equations (MoDEEs) is inspired by our mode decomposition via iterative filtering,^{41,70} which is equivalent to the use of high order PDE high-pass filters. MoDEE yields band-frequency components (or modes) by recursively extracting high frequency signals using high order PDEs. The proposed MoDEEs behave like Fourier transform and wavelet transform — the intrinsic modes generated from MoDEEs have a perfect reconstruction of the original function. In this sense, we also call the operation of MoDEEs a PDE transform. However, the proposed PDE transform is capable of decomposing signals and images into various “functional” modes instead of pure frequency modes like those in Fourier transform. By functional modes, we mean the components which share similar band of frequencies or belong to same category, e.g., noise, edge and trend. But unlike wavelet transform, the proposed PDE transform works like a series of low-pass and/or high-pass filters in the spatial or time domain only. As such, the subsequential secondary processing on each individual mode become robust and controllable, leading to desirable processing effects.

The rest of the present paper is organized as follows. Section II is devoted to the theory and algorithm of the proposed PDE transform or MoDEEs. We start with a brief review of high order image processing PDEs and PDE based high-pass filters. MoDEEs are constructed by an appropriate generalization of the PDE based high-pass filters.⁷⁶ A number of MoDEE systems are presented. The n th order MoDEE system involves $2n$ th order PDEs. Computational algorithms are proposed in Section III. As the proposed MoDEEs are coupled nonlinear PDEs involving high order derivatives, their solution is non trivial. We propose many simplified MoDEE systems, including decoupled MoDEEs, linear MoDEEs

and algebraic MoDEEs to reduce computational complexity. The Fourier pseudospectral method^{64,82} is employed to numerically solve MoDEE systems. This approach is exact for certain class of PDEs. Numerical tests and validations are presented in Section IV. A benchmark test is to separate adjacent frequency modes in a function or signal. This test becomes difficult when the adjacent modes are of high frequencies. Other tests include image edge detection, denoising and enhancement. We show that the proposed MoDEEs are able to perform well on all these tests. In Section V, applications of proposed PDE transform are considered to the processing of a few medical images. We demonstrate the performance of the proposed MoDEEs for image denoising, restoration and edge detection. This paper ends with some concluding remarks.

II Theory and formulation

This section presents the theoretical formulation of PDE based mode decomposition methods. To establish notation and illustrate concepts, we briefly review high-order PDE based nonlinear low-pass filters introduced by Wei⁷³ and PDE based nonlinear high-pass filter introduced by Wei and Jia.⁷⁶ The construction of mode decomposition evolution equations (MoDEEs) follows as a natural extension of the PDE based nonlinear high-pass filter.

II.A High order PDE based low-pass filters

Motivated by a number of physical phenomena, such as pattern formation in alloys, glasses, polymer, combustion and biological systems, Wei introduced some of the first family of high order nonlinear PDEs for image processing in 1999⁷³

$$\frac{\partial u(\mathbf{r}, t)}{\partial t} = \sum_q \nabla \cdot [d_q(u(\mathbf{r}), |\nabla u(\mathbf{r}), t) \nabla \nabla^{2q} u(\mathbf{r}, t)] + e(u(\mathbf{r}), |\nabla u(\mathbf{r}, t), t), \quad q = 0, 1, 2, \dots \quad (1)$$

where $u(\mathbf{r}, t)$ is the image function with Neumann boundary conditions imposed, $d_q(u(\mathbf{r}), |\nabla u(\mathbf{r}), t)$ and $e(u(\mathbf{r}), |\nabla u(\mathbf{r}), t)$ are edge sensitive diffusion coefficients and enhancement operator respectively. Equation (1) is a generalization of the Perona-Malik equation,⁵³ where the latter is recovered at $q = 0$ and $e(u(\mathbf{r}), |\nabla u(\mathbf{r}), t) = 0$. The hyperdiffusion coefficients $d_q(u(\mathbf{r}), |\nabla u(\mathbf{r}), t)$ were chosen as

$$d_q(u(\mathbf{r}), |\nabla u(\mathbf{r}), t) = d_{q0} \exp \left[\frac{|\nabla u|^2}{2\sigma_q^2} \right], \quad (2)$$

where the values of constant d_{q0} depend on the noise level, and σ_0 and σ_1 were chosen as the local statistical variance of u and ∇u

$$\sigma_q^2(\mathbf{r}) = \overline{|\nabla^q u - \overline{\nabla^q u}|^2} \quad (q = 0, 1), \quad (3)$$

The notation $\overline{X(\mathbf{r})}$ denotes the local average of $X(\mathbf{r})$ centered at position \mathbf{r} . The statistical measure based on the variance is important for discriminating image edges from noise. By using this measure, one can avoid the use of preprocessing, i.e., the convolution of the noise image with a smooth mask. The numerical application of Eq. (1) to image denoising and restoration was demonstrated and the performance of this equation was compared with that of the Perona-Malik equation⁵³ by Wei⁷³ and many other researchers.^{22,23,43} The well-posedness of the generalized Perona-Malik equation was analyzed in terms of the existence and uniqueness of the solution.^{7,24,25,36,81} It was argued that the mathematical properties of the generalized Perona-Malik equation differ from those of other high order PDEs.³⁶ The stability of Eq. (1) follows from appropriate choice of diffusion coefficients $d_q(u(\mathbf{r}), |\nabla u(\mathbf{r}), t)$, e.g., the sign of d_q should be $(-1)^q$. However, other choices of the signs were also explored in forward-and-backward diffusion processes to achieve simultaneous image denoising and enhancement.²²

II.B Nonlinear PDE based high-pass filters

By 2000, there had been a large number of publications that explored PDE based image processing approaches. However, most of the research was focused on the use of even-order partial derivatives as a means to smooth images, i.e., as low-pass filters. These PDE approaches were inefficient for image edge detection, particularly for images with a large amount of texture. This is due to the fact that edge

detection is a high-pass filtering operation, while the diffusion process is inherently a low-pass filtering process. Wei and Jia addressed this issue by introducing a pair of weakly coupled nonlinear evolution equations in 2002⁷⁶

$$\frac{\partial}{\partial t} u(\mathbf{r}, t) = F_1(u, \nabla u, \nabla^2 u, \dots) + \epsilon_1(v - u) \quad (4)$$

$$\frac{\partial}{\partial t} v(\mathbf{r}, t) = F_2(v, \nabla v, \nabla^2 v, \dots) + \epsilon_2(u - v) \quad (5)$$

where $u(\mathbf{r}, t)$ and $v(\mathbf{r}, t)$ are scalar fields with Neumann boundary conditions imposed, ϵ_1 and ϵ_2 are coupling strengths. F_1 and F_2 are general nonlinear functions which can be chosen as the Perona-Malik operator

$$F_j = \nabla \cdot [d_j(|\nabla u_j|)\nabla u_j] \quad (6)$$

with $d_j(|\nabla u_j|) = d_{j0} \exp[-|\nabla u_j|^2/(2\sigma^2)]$, $u_1 = u$ and $u_2 = v$. The initial values for both scalar fields were chosen to be the same image of interest, i.e., $u(\mathbf{r}, 0) = v(\mathbf{r}, 0) = I(\mathbf{r})$. In the theory of nonlinear dynamics, Eqs. (4) and (5) constitute a synchronization system. To attain an appropriate image edge contrast, two dynamical systems must differ dramatically in their time scales of motion, i.e., either $d_{10} \gg d_{20}$ or $d_{20} \gg d_{10}$. The coupling strengths ϵ_1 and ϵ_2 were set to be relatively small (i.e., $\epsilon_1 \cong \epsilon_2 \sim 0$) so that the rate of change of u or v was dominated by the diffusion process. The image edge was defined as the difference of two dynamical systems

$$w(\mathbf{r}, t) = u(\mathbf{r}, t) - v(\mathbf{r}, t). \quad (7)$$

To ensure a normal performance of diffusion operator, one of the diffusion coefficients d_{10} or d_{20} must be of similar amplitude as that used in the Perona-Malik dynamics. If we choose d_{20} to be a normal one, the requirement of $d_{20} \gg d_{10}$ implies that $d_{10} \approx 0$. Therefore we have another expression for the PDE based edge function

$$w(\mathbf{r}, t) = I(\mathbf{r}) - v(\mathbf{r}, t). \quad (8)$$

This setting is often used in our practical applications.^{64,65} The PDE based high-pass filters have been shown to be very robust and efficient. They provide superior results in image edge detection compared to those obtained by using other existing approaches, such as the Sobel, Prewitt, and Canny operators, and by anisotropic diffusion.⁷⁶

II.C Mode decomposition evolution equations (MoDEEs)

The high-pass PDE filter discussed above does not discriminate different high frequency modes or components. The goal of the proposed project is to devise a PDE based system for systematic separation of all the mode components, including high order modes. This requires a generalization of the PDE based high-pass PDE filter. To this end, we first cast Eqs. (4) and (5) into a matrix form

$$\frac{\partial}{\partial t} \begin{pmatrix} u \\ v \\ w \end{pmatrix} = \begin{pmatrix} \nabla \cdot d_u(|\nabla u|)\nabla - \epsilon_1 & \epsilon_1 & 0 \\ \epsilon_2 & \nabla \cdot d_v(|\nabla v|)\nabla - \epsilon_2 & 0 \\ \nabla \cdot d_u(|\nabla u|)\nabla - (\epsilon_1 + \epsilon_2) & -\nabla \cdot d_v(|\nabla v|)\nabla + (\epsilon_1 + \epsilon_2) & 0 \end{pmatrix} \begin{pmatrix} u \\ v \\ w \end{pmatrix}, \quad (9)$$

where all quantities are same as those defined in the last section. Considering the fact that $w = u - v$ and $\epsilon_1 \cong \epsilon_2 \sim 0$, we can arrive at a more compact form

$$\frac{\partial}{\partial t} \begin{pmatrix} u \\ v \\ w \end{pmatrix} = \begin{pmatrix} \nabla \cdot d_u(|\nabla u|)\nabla & 0 & -\epsilon_1 \\ 0 & \nabla \cdot d_v(|\nabla v|)\nabla & \epsilon_2 \\ \nabla \cdot d_u(|\nabla u|)\nabla & -\nabla \cdot d_v(|\nabla v|)\nabla & 0 \end{pmatrix} \begin{pmatrix} u \\ v \\ w \end{pmatrix}, \quad (10)$$

where the coupling strengths $(\epsilon_1 + \epsilon_2)$ in the evolution equation of w has been dropped for simplicity. Equation system (10) is hereafter referred to as the *first MoDEE system*.

Note that the PDE for “edge” w in Eq. (10) is very different from the other two genuine PDEs for u and v . The solution of w is easily obtained by integrating the corresponding PDE once only, provided that u and v are given.

For problems involving high frequency modes, we need to construct high order MoDEEs. The matrix form (10) can be easily generalized to include fourth order derivatives

$$\frac{\partial}{\partial t} \begin{pmatrix} u \\ v_1 \\ v_2 \\ w_1 \\ w_2 \end{pmatrix} = \begin{pmatrix} \nabla \cdot d_u(|\nabla u|)\nabla & 0 & 0 & 0 & -\epsilon_1 \\ 0 & \nabla \cdot d_1(|\nabla v_1|)\nabla & 0 & 0 & \epsilon_2 \\ 0 & 0 & \nabla \cdot d_2(|\nabla v_2|)\nabla\nabla^2 & 0 & -\epsilon_3 \\ \nabla \cdot d_u(|\nabla u|)\nabla & -\nabla \cdot d_1(|\nabla v_1|)\nabla & 0 & 0 & 0 \\ \nabla \cdot d_u(|\nabla u|)\nabla & -2\nabla \cdot d_1(|\nabla v_1|)\nabla & \nabla \cdot d_2(|\nabla v_2|)\nabla\nabla^2 & 0 & 0 \end{pmatrix} \begin{pmatrix} u \\ v_1 \\ v_2 \\ w_1 \\ w_2 \end{pmatrix}, \quad (11)$$

where the differential equation of v_2 is a fourth order nonlinear low-pass filters. Here w_2 is more sensitive to high frequency components than w_1 is. Therefore, w_2 contains the information related to the difference between high order modes. As discussed earlier, it is computationally cheaper to solve edge functions w_1 and w_2 than to solve v_1 and v_2 . We have utilized the fourth order operator designed by Wei⁷³ in the above formulation. The initial values of u, v_1 and v_2 are set to the original image or signal of interest. The initial value of w_1 and w_2 can be set to zero. Equation system (11) is hereafter referred to as the *second MoDEE system*.

Similar to the first MoDEE system, the second MoDEE system works when one sets $d_{u0} \sim 0$ and $\epsilon_j \sim 0$ ($j = 1, 2, 3$). If the task is merely to detect image edges, one may just use the first MoDEE system to obtain desirable results as demonstrated in our earlier work.^{64,76} However, if one wants to separate high frequency modes, the second MoDEE system is a better candidate than the first one. For highly oscillatory signals, images and functions, in order to separate all the high frequency modes, which is desirable in many applications, we need MoDEE containing even higher order PDEs. To this end, we construct an n th order system. Let us denote $\mathbf{u} = (u, v_1, \dots, v_n, w_1, \dots, w_n)^T$ which is a $(2n + 1)$ -component state vector. Here u is essentially a copy of the initial image function or signal, v_1, \dots, v_n are essentially copies of the smoothed versions of u , and w_1, \dots, w_n are n edge functions. We can write out the general form for the n th MoDEE system as follows:

$$\frac{\partial}{\partial t} \mathbf{u} = \mathbf{F}\mathbf{u}, \quad (12)$$

where \mathbf{F} is a $(2n + 1) \times (2n + 1)$ matrix. On the first row of \mathbf{F} , the only non-zero matrix elements are $\mathbf{F}_{1,1} = \nabla \cdot d_u(|\nabla u|)\nabla$ and $\mathbf{F}_{1,2n+1} = -\epsilon_1$. For rows $i = 2, \dots, n + 1$, the non-zero matrix elements are given by $\mathbf{F}_{i,i} = \nabla \cdot d_{i-1}(|\nabla v_{i-1}|)\nabla\nabla^{2(i-1)}$ and $\mathbf{F}_{i,2n+1} = (-1)^i \epsilon_i$. For the rest n rows with row index $i = n + 2, \dots, 2n + 1$, matrix elements in the first column are given by $\mathbf{F}_{i,1} = \nabla \cdot d_u(|\nabla u|)\nabla$, and those in column j , where $2 \leq j \leq i - n$, are given by

$$\mathbf{F}_{i,j} = (-1)^{j-1} \binom{i - (n + 1)}{j - 1} \nabla \cdot d_{j-1}(|\nabla v_{j-1}|)\nabla\nabla^{2(j-1)} \quad (13)$$

and all other terms are set to zero. In Eq. (13), $\binom{m}{l} = \frac{m!}{l!(m-l)!}$ is the binomial coefficient. The choice of the binomial coefficient is inspired by the structure of our iterative filtering operator.^{41,70} Equation (12) can be solved to generate n edge functions $w_j(\mathbf{r}, t)$ ($j = 1, 2, \dots, n$). These edge functions correspond to intrinsic mode functions from another perspective. The Neumann boundary condition can be used in all the proposed MoDEEs.

III Simplified models and computational algorithms

III.A Linear MoDEEs

In general, we need to solve systems of coupled, nonlinear, high order PDEs as shown in Eq. (12), which can be technically demanding. However, for many practical problems, we can design simplified MoDEE models which also work well. Based on the physical understanding, various simplifications of

the MoDEE systems are presented to reduce the computational complexity. Numerical algorithms for solving high order MoDEEs are also discussed in the following paragraphs.

The first approximation is to set $\epsilon_j = 0$ in MoDEEs. This approximation leads to the decoupling of all MoDEEs. The uncoupled MoDEEs are much easier to solve. The solutions of decoupled PDEs are also easy to interpret, which makes the selection of mode parameters easy.

Another useful approximation is to eliminate nonlinearity and positional dependence of all the diffusion coefficients. The nonlinear models work better for most application as evident from our own experiments. However, for certain class of problems with smooth functions, the nonlinear edge sensitive diffusion coefficients do not play the critical role. Therefore, linear MoDEE systems are computationally favored. As an example, we can obtain a linear form of the second MoDEE system from Eq. (11):

$$\frac{\partial}{\partial t} \begin{pmatrix} u \\ v_1 \\ v_2 \\ w_1 \\ w_2 \end{pmatrix} = \begin{pmatrix} d_0 \nabla^2 & 0 & 0 & 0 & 0 \\ 0 & d_1 \nabla^2 & 0 & 0 & 0 \\ 0 & 0 & d_2 \nabla^4 & 0 & 0 \\ d_0 \nabla^2 & -d_1 \nabla^2 & 0 & 0 & 0 \\ d_0 \nabla^2 & -2d_1 \nabla^2 & d_2 \nabla^4 & 0 & 0 \end{pmatrix} \begin{pmatrix} u \\ v_1 \\ v_2 \\ w_1 \\ w_2 \end{pmatrix}, \quad (14)$$

where d_j ($j = 0, 1, 2$) are constants such that $d_1 > |d_2| \gg d_0 \sim 0$. All the other MoDEE systems can be similarly simplified. Linear MoDEE systems can be easily solved with the Fourier spectral methods.^{65,82}

III.B Algebraic MoDEEs

To further simplify MoDEE systems, we can make use of the algebraic relation given in the original formulation of Wei and Jia.⁷⁶ The use of algebraic relations saves the computational cost of integrating the edge equations. We first consider a set of linear equations as those given in Eq. (14)

$$\frac{\partial}{\partial t} \begin{pmatrix} v_1 \\ v_2 \\ v_3 \\ \vdots \\ v_n \end{pmatrix} = \begin{pmatrix} d_1 \nabla^2 & 0 & 0 & \cdots & 0 \\ 0 & d_2 \nabla^4 & 0 & \cdots & 0 \\ 0 & 0 & d_3 \nabla^6 & \cdots & 0 \\ \vdots & \vdots & \vdots & \cdots & \vdots \\ 0 & 0 & 0 & \cdots & d_n \nabla^{2n} \end{pmatrix} \begin{pmatrix} v_1 \\ v_2 \\ v_3 \\ \vdots \\ v_n \end{pmatrix} \quad (15)$$

These linear equations offer n copies of smoothed image functions. After an appropriate choice of d_1 , other coefficients can be set as $d_j = (-1)^{j-1} d_1^j$ ($j = 2, 3, \dots$). After solving Eq. (15) for state vector \mathbf{v} , we need to determine the mode vector $\mathbf{w} = (w_1, w_2, w_3, \dots, w_n)^T$, which can be constructed through the following algebraic relations

$$\begin{pmatrix} w_1 \\ w_2 \\ w_3 \\ w_4 \\ \vdots \\ w_n \end{pmatrix} = \begin{pmatrix} 1 & -1 & 0 & 0 & 0 & \cdots \\ 1 & -2 & 1 & 0 & 0 & \cdots \\ 1 & -3 & 3 & -1 & 0 & \cdots \\ 1 & -4 & 6 & -4 & 1 & \cdots \\ \vdots & \vdots & \vdots & \vdots & \vdots & \vdots \\ \vdots & \vdots & \vdots & \vdots & \vdots & \vdots \end{pmatrix} \begin{pmatrix} u \\ v_1 \\ v_2 \\ v_3 \\ \vdots \\ v_n \end{pmatrix}, \quad (16)$$

where $u(\mathbf{r}) = I(\mathbf{r})$ is set to the initial image function or signal and the matrix is of $n \times (n+1)$ dimensions. The matrix elements are binomial coefficient as those in Eq. (13). However, for a given w_j , there are other ways to select the combination of lower order derivative terms.

A different approach is to construct a mode vector \mathbf{w}' by the simple form as that given in Eq. (8)

$$w'_j(\mathbf{r}, t) = I(\mathbf{r}) - v_j(\mathbf{r}, t), \quad j = 1, 2, \dots, n. \quad (17)$$

We expect that \mathbf{w}' behaves similar to \mathbf{w} does. Obviously, there are still many other ways to construct mode vectors. Essentially, for a given application, the selection of appropriate v_k , ($k < j$) for the construction of j th order of mode component w_j can be formulated as an optimization problem. It is beyond the scope of the present work to discuss other alternative MoDEEs.

III.C Numerical methods for high-order MoDEEs

The proposed MoDEEs involve many high order PDEs which have to be solved in an appropriate manner to avoid the accumulation of numerical errors. Essentially, there are two important issues in the solution of high order evolution PDEs. The first issue concerns the accuracy of approximating high order derivatives. The rule of thumb here is that to approximate high order derivatives, high order numerical methods are required.^{71,86} High order finite difference methods based on the Lagrange polynomials, Fourier pseudospectral methods and local spectral methods are suitable approaches for approximating high order derivatives. The second issue is the stability constraint in solving high order evolution PDEs. When the explicit (forward) Euler type of time discretization is used to solve an n th order evolution PDE, the step size Δt of time is constrained by $\Delta t \sim (\Delta x)^n$, where Δx is the spatial grid spacing. Therefore, it is desirable to use alternative direction implicit (ADI) type of implicit methods for the time discretization. ADI type of methods has been previously developed by us to solve geometric flow equations.^{5,18}

To solve decoupled linear MoDEEs (15), we use the Fourier pseudospectral method. Spectral methods have been a popular choice for the numerical solution of various wave problems in recent years. As global methods, the Fourier spectral methods usually are much more efficient than local methods (e.g., finite difference and finite element methods) for certain classes of nonlinear problems. We applied Fourier pseudospectral method to the solution of the Navier-Stokes equation and other PDEs.^{65,82} A windowed Fourier pseudospectral method has been developed for hyperbolic conservation laws, i.e., Euler equations.⁶⁵ This approach is unconditionally stable and particularly efficient for solving high order MoDEEs proposed in Eq. (15).

IV Numerical tests and validations

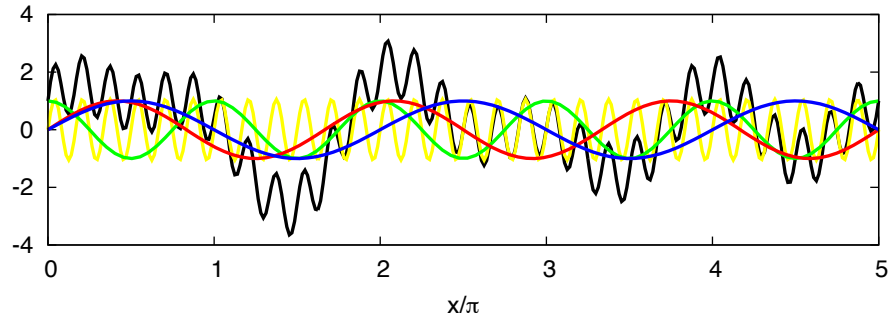
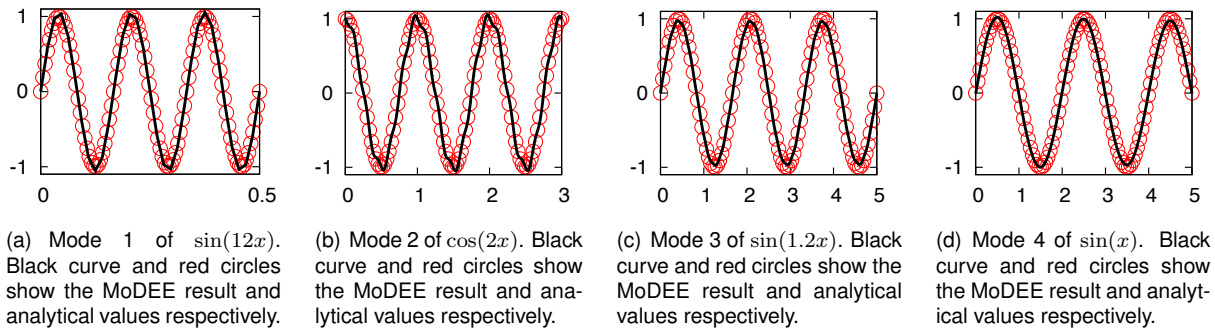
IV.A Intrinsic mode decomposition

In this section, MoDEE is applied to and validated on several benchmark testing cases to demonstrate the flexibility, efficiency, and accuracy of the method. In this paper, we use local spectral evolution kernel to numerically calculate PDEs encountered in the MoDEE scheme.^{70,84}

We first illustrate the efficiency and accuracy of the MoDEE algorithm III.B using signal $f(x) = \sin(x) + \sin(1.2x) + \cos(2x) + \sin(12x)$, as shown in Figure 1(e). In the figure, x-axis is in the range of $(0, 5\pi)$. The total signal $f(x)$ is shown in solid black curve, and the four frequency modes are plotted with yellow, green, red and blue solid curves respectively. MoDEE decomposes the total signal into four modes which agree very well with the analytical results. For a detailed comparison, MoDEE results and analytical modes are plotted together for comparison in Figures 1(a), 1(b), 1(c) and 1(d) respectively. Note that mode 3 of $\sin(1.2x)$ and mode 4 of $\sin(x)$ are closely embedded in $f(x)$ and are thus difficult to be separated using many methods other than Fourier transform or wavelet methods. MoDEE method illustrates its advances in separating out various modes clearly. The signal here is perfect candidate for application of Fourier method, and MoDEE gives satisfactory decomposition accurately. It is desirable to make further detailed analysis using this example.

In Figure 2, a comparison and study of the effect of high order PDEs are illustrated. Mode 1 of $\sin(12x)$ is plotted in the Figure. Red curves in three panels show the result using MoDEE method with different highest order of PDEs, and black curves show the analytical results of $\sin(12x)$ as reference. The value n , which is the highest order of PDE as in ∇^{2n} in Eq. (15), are 1, 2 and 4 respectively. For this mode, use of up to 4th-order (i.e. $n = 2$) PDE term is enough for the convergence of MoDEE method. Similar plots of the decomposition of the third mode $\sin(1.2x)$ from the fourth one $\sin(x)$ are shown in Figure 3. Even when $n = 10$ is used, discrepancy between MoDEE and analytical results is still quite large (shown in the middle panel of the figure). High order PDEs up to as large as $n = 40$ are used in MoDEE. The results illustrate how important it is and when it is necessary to include very high order PDEs for signal processing. In addition, it is shown that MoDEE using very high order PDEs is still very stable and does not diverge.

The second example is the signal $f(x) = \sin(x) + \sin(1.2x) + \cos(2x) + \eta_1(x) + \eta_2(x)$ (shown in Figure 4(a)), where $\eta_1(x)$ and $\eta_2(x)$ are Gaussian white noise with different frequencies (shown in Figures 4(b) and 4(c) respectively). The frequency of $\eta_1(x)$ is the highest one which can be supported by the grid meshes, while $\eta_2(x)$ oscillates with frequency four times smaller (or slower).



(e) Black curve shows the signal $f(x) = \sin(x) + \sin(1.2x) + \cos(2x) + \sin(12x)$. X-axis is in the unit of π and range of $(0, 5\pi)$ is used in the above plot. Yellow, green, red and blue curves are the four modes, $\sin(12x)$, $\cos(2x)$, $\sin(1.2x)$ and $\sin(x)$, separated from $f(x)$ using MoDEE method. The four modes agree very well with the corresponding analytical values, as shown in Figures 1(a), 1(b), 1(c) and 1(d) respectively. Note that mode 3 of $\sin(1.2x)$ and mode 4 of $\sin(x)$ are closely embedded in $f(x)$ and are thus difficult to be separated.

Figure 1: Mode separation using MoDEE method.

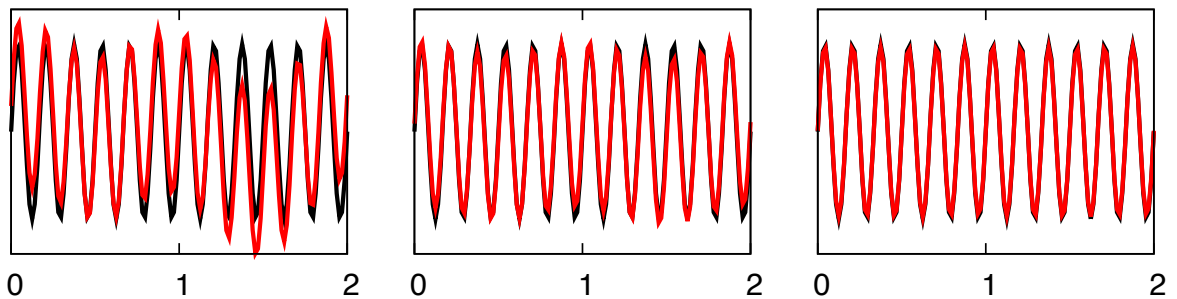


Figure 2: Mode 1 of $\sin(12x)$. Red curves in three panels show the result using MoDEE method with different highest order of PDEs, and black curves show the analytical results of $\sin(12x)$ as reference. The value n of highest order in ∇^{2n} are 1, 2 and 4 respectively. For this mode, use of up to 4th-order (i.e. $n = 2$) PDE term is enough for the convergence of MoDEE method.

There are two challenges in decomposing signals into frequency modes and noises. First of all, the frequency modes, especially $\sin(x)$ and $\sin(1.2x)$ are very close in frequency domain. In addition, the signal is mixed with two white noises, which have large amplitude and are composed of two different frequencies. In Figure 5, effects of high order PDEs are studied by varying value of n as in ∇^{2n} . In Figures 5(a), 5(b) and 5(c), $n = 1, 10, 30$ are used respectively. In each of the three figures, high frequency noise $\eta_1(x)$ is plotted in the upper panel, while the corresponding residue $f(x) - \eta_1(x)$ being plotted in the lower panel. In all the figures and panels, exact values of $\eta_1(x)$ (which was recorded when it was randomly generated initially) are plotted in green color, and MoDEE results are plotted

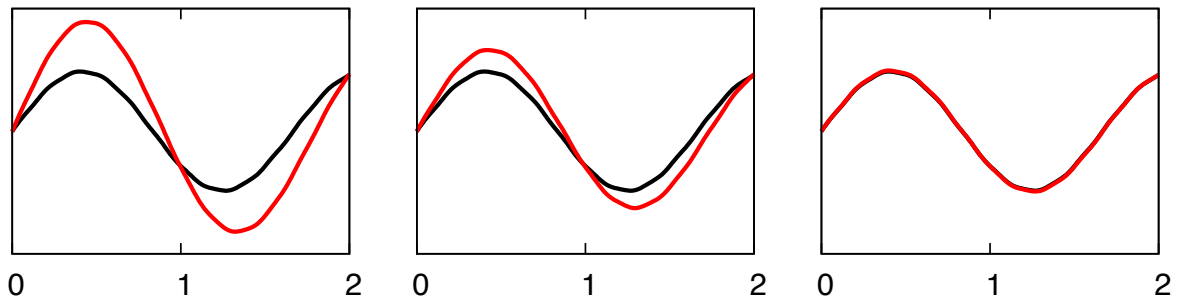
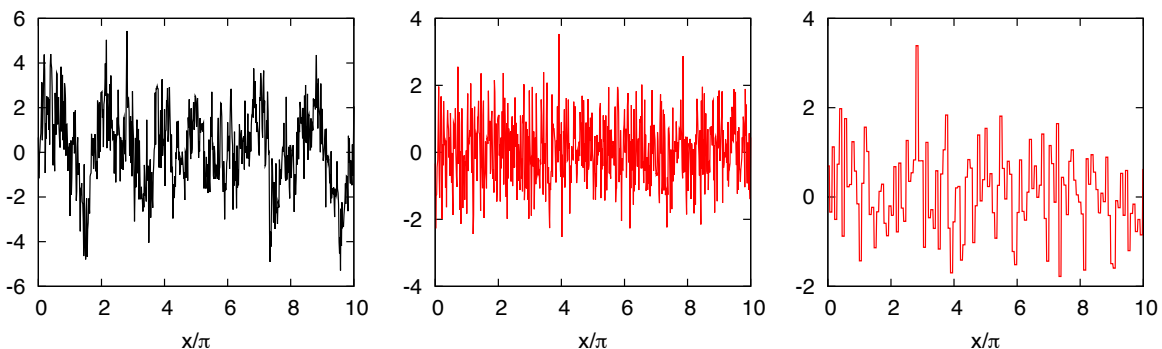


Figure 3: Mode 3 of $\sin(1.2x)$. Since this mode is very close to mode 4 of $\sin(x)$, high order PDE term is needed. In the panels from left to right, the highest order of PDE is $n = 1, 10, 40$ respectively. Red curves show the MoDEE result and black curves show the analytical plot of $\sin(1.2x)$ as reference. A very high order of $n = 40$ is necessary for the convergence of MoDEE method. On the other hand, MoDEE remains quite stable when high order PDE is used.



(a) Signal $f(x) = \sin(x) + \sin(1.2x) + \cos(2x) + \eta_1(x) + \eta_2(x)$. (b) High frequency white-noise $\eta_1(x)$. (c) Lower frequency white-noise $\eta_2(x)$.

Figure 4: Modes detection and noises removal for signal composed of various closely embedded two-mode noise and three-mode oscillation.

in red color. A clear trend in the accuracy improvement is observed with the increase of value of n . Finally, the three components of $\sin(x)$, $\sin(1.2x)$ and $\cos(2x)$ in $f(x)$ are plotted in Figure 6. In Figure 6(a), the original signal $f(x)$ including noises is plotted with black solid line, while the noise-free signal $f'(x) = \cos(2x) + \sin(1.2x) + \sin(x)$ is plotted with red solid lines for reference. The three non-noise modes are plotted in black, red, and blue curves respectively in Figure 6(b). For each mode, numerical results (solid lines) are compared with analytical ones (circles). Once again, a very good matching between MoDEE calculation and exact values is achieved.

Lastly, we illustrate the spectral accuracy achieved by MoDEE using signal composed of two modes of $\cos(mx)$ and $\cos((m-1)x)$, where m is the maximum frequency that can be supported by the mesh size (which is 0.05 in this example, and thus $m = 20$), i.e. two grid points for each oscillation period. In Figure 7, $f(x) = \cos(mx) + \cos((m-1)x)$ is decomposed into the two frequency modes, $\cos(mx)$ and $\cos((m-1)x)$, using MoDEE. The plots for the two modes are shown in Figures 7(a) and 7(b) respectively. Black curve shows the total signal $f(x)$, red curve and blue circle show the exact and MoDEE results respectively. Highly accurate MoDEE decomposition is observed in the figures using high order PDE with $N = 100$ in MoDEE algorithm given in section III.A.

IV.B Image denoising, edge detection and enhancement

Image processing is becoming increasingly important in many areas of research in physical, mathematical and biological sciences.^{16,28,29,39,55} In particular, edge detection is a key issue in pattern recognition, computer vision, target tracking and image processing.^{2,3,9,49,59,61} Closely related to edge detection is denoising. PDE methods provide powerful image processing tools. MoDEE is designed for both accu-

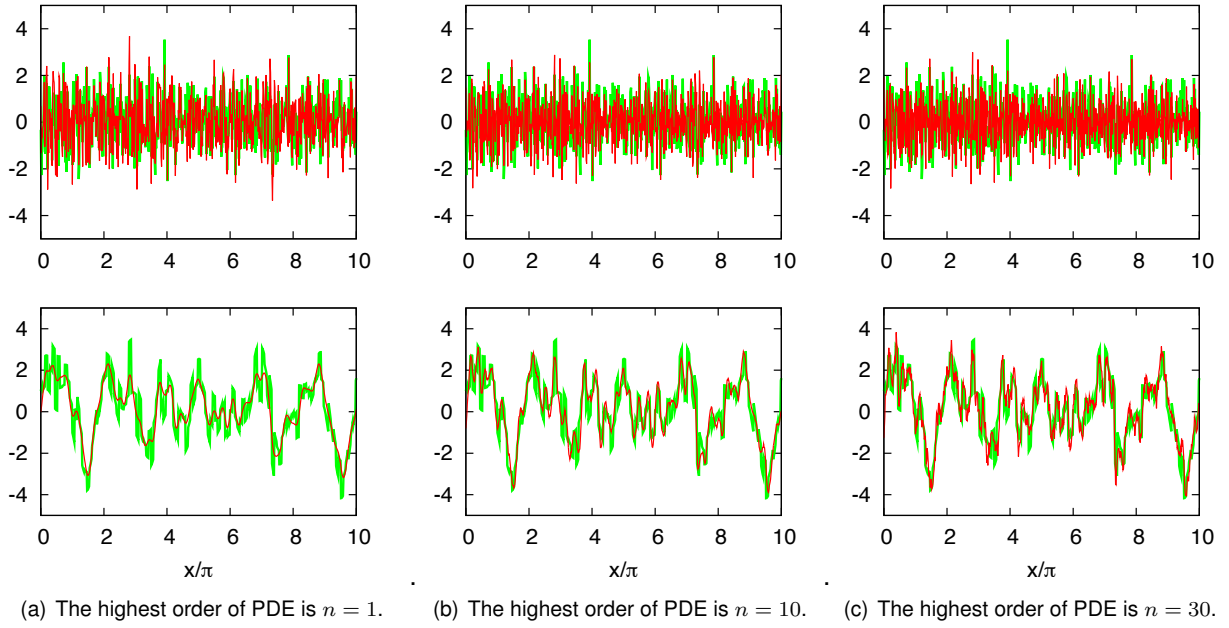


Figure 5: Separation of high frequency noise from low frequency noise and signal using MoDEE method. In each of the Figures 5(a), 5(b) and 5(c), exact values (green solid line) and MoDEE results (red solid line) of high frequency noise $\eta_1(x)$ are shown in the upper panels, while plots showing the original signal minus the high frequency noise are shown in the lower panels. It is observed that use of higher order PDEs leads to better results of the high frequency noise $\eta_1(x)$.

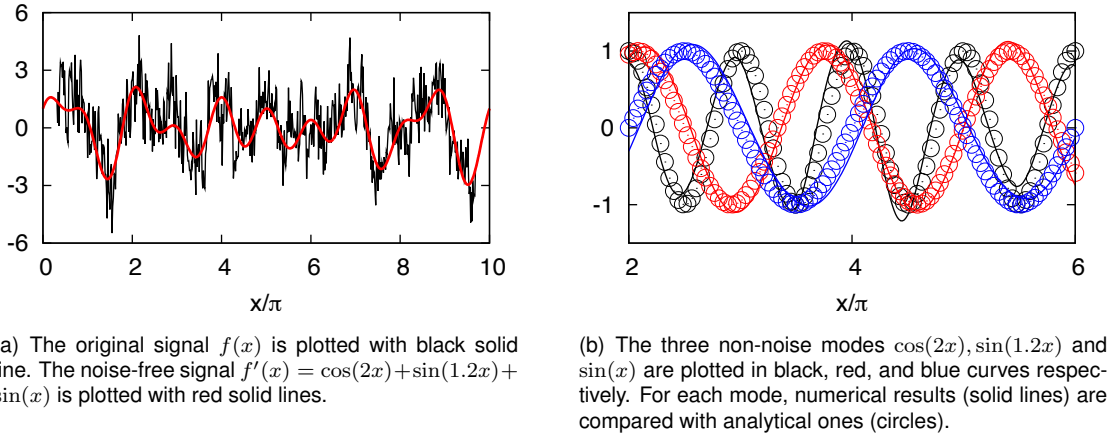
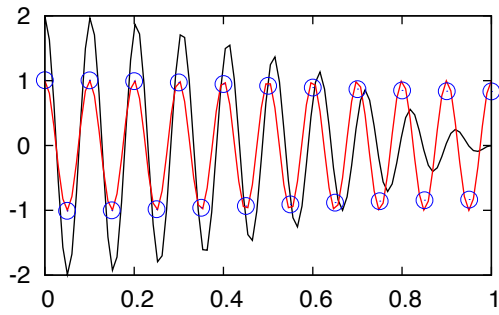


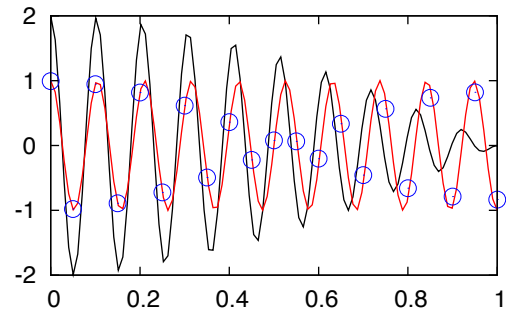
Figure 6: Plots of noises, noise-free signals, and modes extracted using MoDEE.

rately decomposing modes with different frequency (or "frequency-modes") with spectral accuracy and effectively decomposing modes with different functions (of "functional-modes") for image enhancement like edge detection, denoising, segmentation, etc.

In this section, we choose the 512 by 512 grey-scale Barbara.tiff image (Figure 8(a)) for example. The same image has been extensively used in the literature due to its fine details associated with multiple edges. In Figure 8(b) random white Gaussian noise with signal to noise ratio (SNR) of 9.8dB was added to the original image In Figure 8(a). To quantitatively view the noise level as well as to analyze the effect of PDE on the evolution (i.e. processing) of the image, we choose a horizontal line, as plotted by a black line in Figure 8(a), along which the values of grey scale are plotted as shown in Figure 9. The black



(a) Comparison of exact and MoDEE results for the mode $\cos(mx)$.

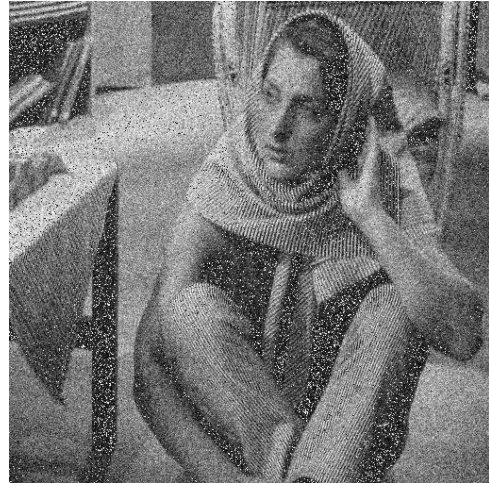


(b) Comparison of exact and MoDEE results for the mode $\cos((m-1)x)$.

Figure 7: Plots of $f(x) = \cos(mx) + \cos((m-1)x)$ where $m = 20$ is the maximum number corresponding to the highest frequency supported by the currently chosen finite grid mesh size. In each subfigure, black curve shows the total signal $f(x)$, red curve and blue circle show the exact and MoDEE results respectively.



(a) Barbara image used for edge and noise analysis. For a detailed analysis, values of grey scale are plotted along the horizontal line as indicated by the black line in the above image.



(b) Random white Gaussian noise is added to the image of Barbara. Signal-to-noise ratio is 9.8dB.

Figure 8: Noise removal using MoDEE.

curve shows the grey scale values along the horizontal line in the original Barbara image, and the red curve shows the grey scale of the same horizontal line (in terms of the value of y-axis in the image) in the noise-added Barbara image 8(b). The added noises overlap closely with the edges of the original image, such that any denoising would smear the fine details of edges.

In Figure 10 results of applying diffusion equation $u_t = D\nabla^2 u$ are shown and compared by using $d_1 = 0.08$ (for upper panel in Figure 10) and $d_2 = 0.4$ (for lower panel in the figure) respectively. Same evolution time of $\Delta t = 10$ is used throughout this paper for image processing, unless otherwise addressed. As expected, heat equation with smaller diffusion constant preserves more edge details together with embedding oscillating noises, while the same PDE with larger d_2 smears out edges while smoothing noises. Such a problem has been well known in image processing, and various variational methods and nonlinear operators have been introduced to preserve more edge details while smoothing the whole image with noises.

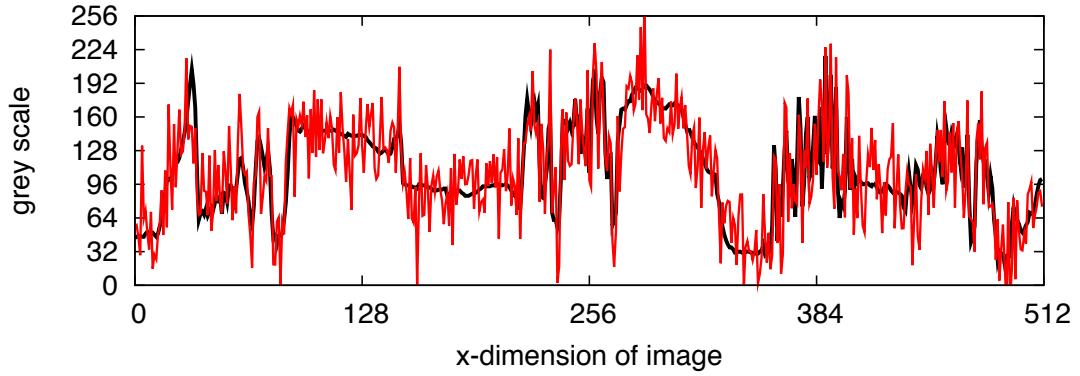


Figure 9: Plot of values of grey scale along the horizontal line highlighted in Figure 8(a). The black and red curve show the grey scale in the original Figure 8(a) and noise image 8(b) respectively.

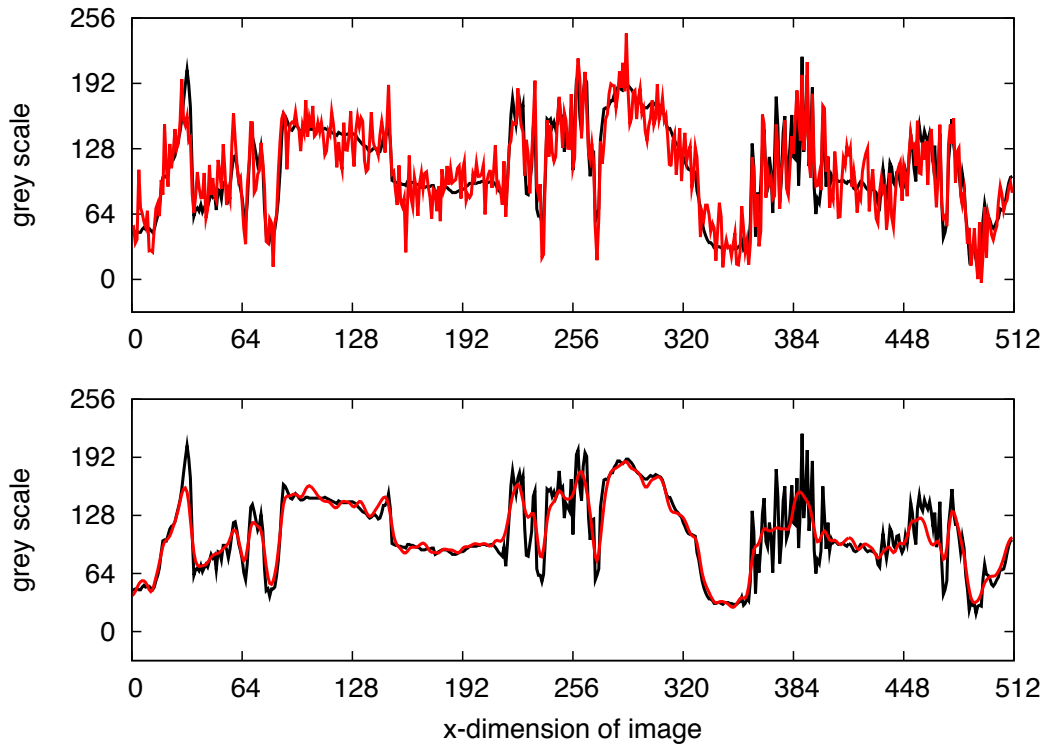
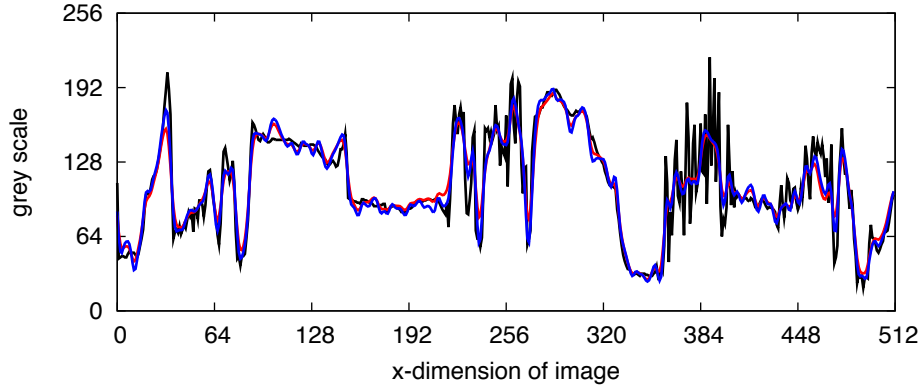
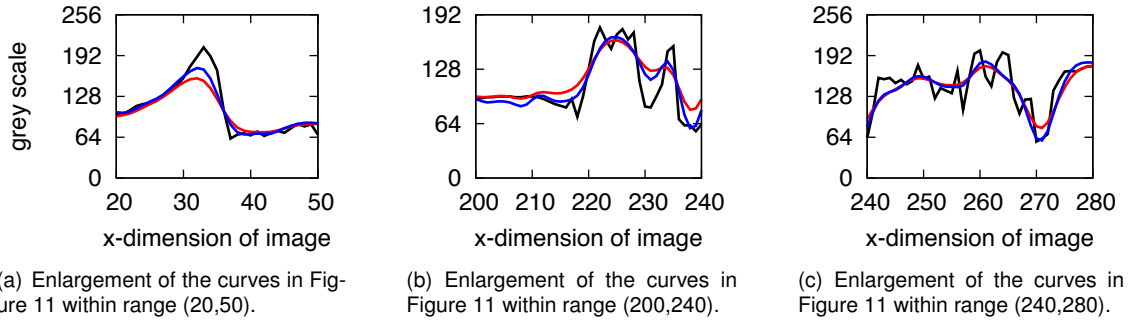


Figure 10: Denoising using diffusion PDE only. The reference black curves show the grey scale values for the horizontal line in the un-noised original Barbara image in Figure 8(a). The red curves show the grey scale for the same horizontal line when diffusion PDE is applied to the noised image. The diffusion constant used to generate the red curve in the upper panel is smaller than that in the lower panel.

MoDEE provides a different approach to the issue from the previous methods. By taking difference between two PDEs with different diffusion constant and inclusion of high order PDEs, namely by applying MoDEE algorithm in III.A to the image, a better denoised image with more edge details can be obtained. In Figure 11, we compare the values of grey scale along the same horizontal line (the black line in Figure 8(a)) obtained by applying diffusion equation with d_2 and MoDEE algorithm III.A. Grey scale of the original clear image is plotted with black curve, and the values obtained as a result of applying diffusion equation with d_2 and MoDEE algorithm III.A are plotted with red and blue curves respectively. In Figure 11(d), values of grey scale in the whole range $x \in [0, 512]$ are plotted. For clearer inspection and comparison, several regions along the x-axis are picked and enlarged to be shown in Figures 11(a), 11(b)



(d) Comparison of methods of single diffusion PDE and MoDEE. Black curve shows the grey scale of the original reference Barbara image along the chosen horizontal line. Red and blue curves show the grey scale of the denoised image using diffusion PDE and MoDEE respectively.

Figure 11: Noise removal using MoDEE.

and 11(c) respectively. The blue curve clearly captures the edge details better than the red curve does, which indicates that MoDEE using high order differentiation and differences between coupled PDEs achieves better separation (through both the scheme itself and more robust choices of parameters) of noises from edges. For visual comparison and appreciation, denoised images using diffusion equation with d_2 and MoDEE are shown in Figure 12. SNR is improved from 16.9dB in Figure 12(a) to 17.4dB in 12(a). Though the improvement in SNR alone is not very big, the visual enhancement is more significant due to the improvement in the fine edge details, i.e. contribution of MoDEE to the visual distinction is bigger than that to the SNR value.

Finally, we explore one more subtle aspect of edge detection and image enhancement using MoDEE. As aforementioned, MoDEE is a very general scheme allowing calculation (or feature extraction) and manipulation of multiple functional modes, each of which possesses specific physical meaning by design. Here we illustrate one such functionality of MoDEE algorithm by adding an additional low pass filter operation to the difference image $u - v$, i.e. $E_1 = \hat{L}_E(\hat{L}_1 u - \hat{L}_2 v)$, where \hat{L} is symbol for general low pass filter. The image E_1 thus obtained is similar to the "residue" image obtained using EMD or IFD algorithm.⁷⁰ Figure 13(a) shows the edge-detection for Barbara using MoDEE algorithm in III.A with (16), and Figure 13(b) is obtained using similar algorithm except that additional post-processing of smoothing is used. Comparing the two figures, it can be observed that edges in Figure 13(a) are finer and sharper, representing good edge extraction. On the other hand, edges in Figure 13(b) have varying density and look more natural to human vision with more physical features captured in detail, e.g. the shade on the elbow of the left hand of Barbara. Rather than edge extraction, edges in Figure 13(b) can be seen as an edge representation, where stronger and more meaningful edges are shown as denser lines while



(a) Denoising using diffusion PDE corresponding to the grey scale of red curve in Figure 11 with signal to noise ratio of 16.9dB.



(b) Denoising using MoDEE corresponding to the grey scale of blue curve in Figure 11 with signal to noise ratio of 17.4dB.

Figure 12: Noise removal using MoDEE.

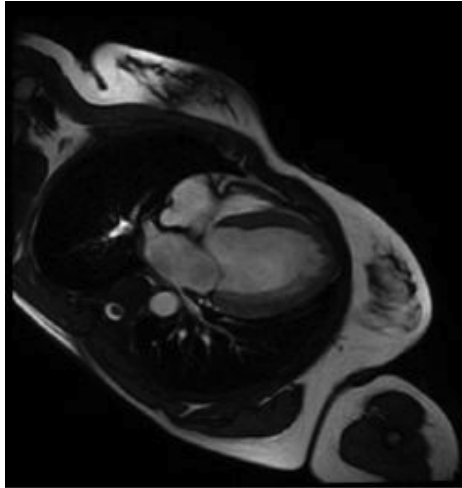


(a) Edge-detection as generated in image E_1 using MoDEE algorithm in III.A. All the fine details are caught in the edge mode. Lines are fine and continuous characterized as good edge detection.



(b) Additional post-processing of smoothing is performed. Lines look natural with various density and width, e.g. the shade on the elbow of the left hand of Barbara. Rather than identified as edge extraction, this image represents the cartoon-like edge mode which differs from finer edges depicted in Figure 13(a).

Figure 13: Edge detection using MoDEE.



(a) Cardiac magnetic resonance imaging (cMRI) for a 21-year-old woman referred for clinical management of idiopathic dilated cardiomyopathy.



(b) Edge detection using MoDEE algorithm (9).

Figure 14: Edge detection and registration using MoDEE.

more subtle edges are shown as finer lines. In many applications this representation may prove to be very useful. This case further justifies the viewpoint proposed in this paper that PDE methods using currently proposed MoDEE algorithms can perform most image processing functions like all the other conventional methods.

V Applications

In the past two decades advances in medical imaging using magnetic resonance imaging (MRI) or computed tomography (CT) technology have enabled both clinicians and researchers to collect and analyze large collection of medical images. In this section, MoDEE algorithm is applied to various types of medical images.

V.A Magnetic resonance images

MRI is built upon the physical theory of nuclear magnetic resonance (NMR): a nucleon such as proton possesses spin which has value of multiples of $1/2$, and those nuclei with unpaired spins tend to align with the orientation of the externally applied magnetic field. After alignment, high frequency pulses, usually in the range of radio frequency (RF) of MHz, are emitted into a slice plane perpendicular to the external field to excite the aligned spins. RF waves are then turned off such that excited nucleus undergo a relaxation process to resume its original distribution. Different types of biological structures and tissues have different characteristic relaxation time which can be measured by MRI hardware and software to construct associated spatial images. Using MRI technique, each pulse sequence exploits some specific physical or chemical property of the protons of small, mobile molecules like water and lipids. Therefore, one could depict structural and functional information from living tissue at the sub-millimeter scale.

Though the medical imaging techniques have advanced tremendously in terms of spatial resolution, acquisition speed, and signal-to-noise ratio, medical images thus created still need to be carefully enhanced to account for factors like signal intensity inhomogeneities (i.e. bias fields), noise, and other artifacts. Noise, as one example, in MRI enters the data samples in k-space and competes with the NMR signal due to random fluctuations in the receiving coil electronics and in the patient body. If one considers the important advancement in MRI, the development of function MRI (fMRI)⁸ for brain mapping and diffusion tensor imaging (DTI)^{72,77} to study neural fibers, the amount of noise in the acquisitions, especially the random thermal noise entering MR data in the time domain, limits the performance and usefulness of quantitative MRI diagnostics such as voxel-based tissue classification, extraction of organ shape or tissue boundaries, estimation of physiological parameters like tissue perfusion and contrast

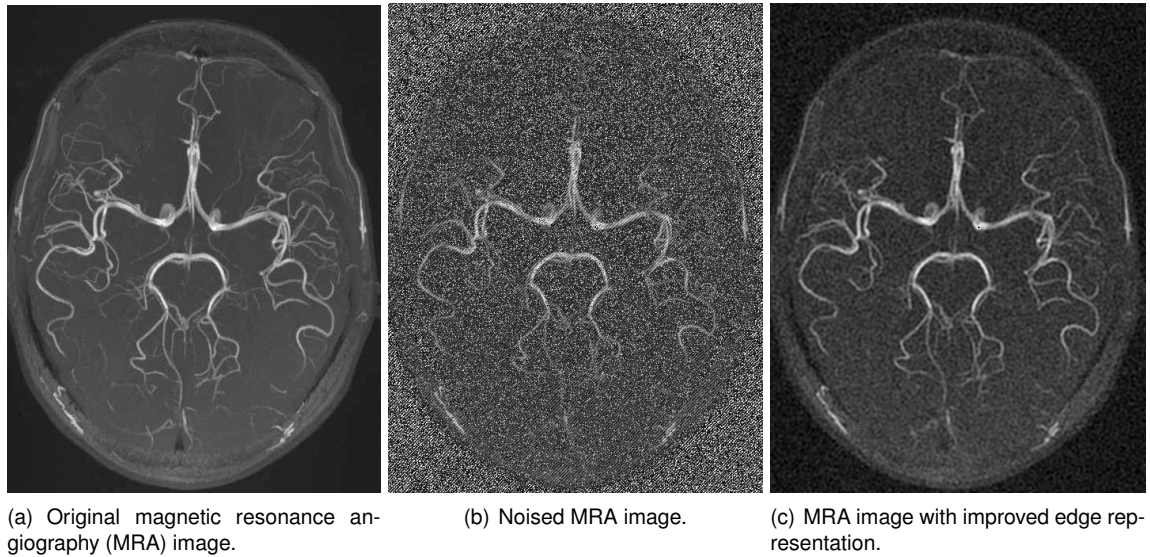


Figure 15: Edge representation in noised image using MoDEE.

agent permeability from dynamic imaging.^{30,43} Despite of the much progress made in post-processing methods for noise reduction and image enhancement, it remains a big challenge and highly desirable to find robust and interacting ways for noise removal, boundary preservation applicable to the different MRI acquisitions techniques.

In Figure 14, the MoDEE algorithm using PDE (9) is used to detect edges for blur medical images obtained using MRI. Figure 14(a) is obtained using cardiac magnetic resonance imaging (cMRI) for a 21-year-old woman referred for clinical management of idiopathic dilated cardiomyopathy. Image is authored by the European society of cardiology. The image shows a dilated left ventricle, without evidence of tissue abnormalities (e.g. scars, patchy fibrosis). With appropriate coefficients chosen in MoDEE algorithm, one can obtain satisfying results showing the effect of edge detection as shown in Figures 16(d) and 14(b) respectively.

V.B Magnetic resonance angiography images

In Figure 15, magnetic resonance angiography (MRA) image is selected for testing and applying the currently proposed MoDEE algorithm. We choose MRA image since it stands for a group of important techniques based on MRI to image blood vessels. The images of the arteries generated by MRA are used to be evaluated for stenosis (abnormal narrowing), occlusion or aneurysms (vessel wall dilatations, at risk of rupture). MRA is often used to evaluate the arteries of the neck and brain, the thoracic and abdominal aorta, the renal arteries, and the legs. An advantage of MRA compared to invasive catheter angiography is the non-invasive character of the examination. In particular, compared to computed tomography and angiography and catheter angiography, MRA does not expose patient to any ionizing radiation. The greatest drawbacks of the method are its comparatively high cost and its somewhat limited spatial resolution. In addition, the length of time the scans take can also be an issue, with computed tomography being far quicker. Therefore, image processing technique is important for post-processing the images generated by MRA to save cost, improve resolution and extract/highlight important features like fine details of edges of arteries.

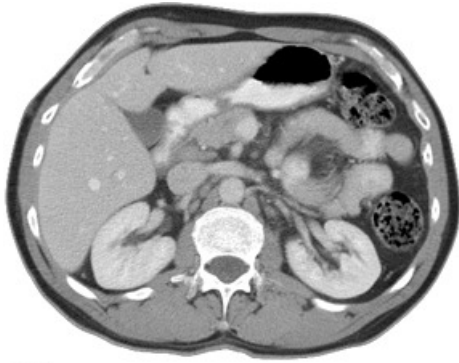
The image shown in Figure 15(a) is downloaded from the website of Magnetic Resonance and Image Analysis Research Centre, University of Liverpool. The image is used to show the vessels known as the Circle of Willis in the brain. To test the ability of edge detection and noise removal, original image is added with noise. For a realistic setting the the total noise added to the MRA image 15(a) is composed of two parts, $\eta(x, y) = \sigma(x, y) + \gamma(x, y)$, where $\sigma(x, y)$ is white Gaussian noise with maximum amplitude



(a) CT image of abdomen of a 68-year old male.



(b) Edge detection using MoDEE algorithm (9).



(c) Cross-sectional image of abdomen using Computerized Axial Tomography (CAT) scanning technique.



(d) Edge detection using MoDEE algorithm (9).

Figure 16: Edge detection and registration using MoDEE.

25 and zero mean, and $\gamma(x, y)$ is a periodically oscillating cosine noise given by

$$\gamma(x, y) = 40 \cos\left(\frac{\pi}{2}(x + y)\right). \quad (18)$$

The noisy image is shown in Figure 15(b). To remove both noises closely embedded in the original image, we apply MoDEE algorithm in Sec. III.A with large enough N (e.g. $N = 20$). The resulting enhanced image is shown in Figure 15(c), in which both types of noises have been greatly reduced and edges are thus clearer for investigation.

V.C X-ray computed tomography images

Computed tomography (CT) is a technology of using X-rays to image biological and human body. Compared to visible spectra imaging, X-rays have wavelengths between nanometer and picometer scales, which are energetic enough to penetrate biological tissues. Denser structures like the bones are more efficient at absorbing X-rays compared to softer tissues. This leads to the noninvasive medical imaging. CT is a popular technique for reconstructing the X-ray images with delicate hardware design as well as computer software. In CT scanning, a localized X-ray source and corresponding detector are put opposite to each other and rotate around the human body. The 2D slice image is then synthesized from the X-ray signals around all the directions. In the last few decades, CT technique has been widely used in medical imaging of soft tissues, hard bonds, blood vessels, etc.

In Figure 16, the MoDEE algorithm using PDE (9), is used to detect edges for medical images obtained using CT. Same set of MoDEE coefficients as in the previous cases are used here, which illustrates the relative stability and robustness of the current methods.

Figure 16(a) shows the CT image of abdomen of a 68-year old male, image authored by Maclennan, Radiologist, Royal Alexandra Hospital, Paisley, United Kingdom. The related report finds calcific density mass, with flat upper margin in neck of gallbladder. The flat margin suggests that whatever is causing the mass is layering under the effect of gravity. The result showing the effect of edge detection is shown in Figure 16(b). Note that fine details of edges are clearly captured, especially those tiny circles corresponding to small dots. Figure 16(c) shows a similar cross-sectional image of abdomen, with image authored by Department of Health and Human Services, using Computerized Axial Tomography (CAT) scanning technique. The two images in Figures 16(a) and 16(c) correspond to different patient with slightly different shapes and organ edges. MoDEE captures the small differences which are reflected in the final edge-extracted modes/images, e.g. the tiny circles in the liver with shapes clearly highlighted. Together with many other possible image enhancements available through MoDEE, both clinical and research scientists can better make use of the medical images generated by CT or MRI techniques.

VI Concluding remarks

Digital image processing, signal processing and video processing underpin a number of modern technologies for optical sorting, automatic control, augmented reality, robotics, sonar, radar, remote sensing, target tracking, communication, navigation and imaging. Mode decomposition is an elementary operation in image and signal processing, and enables essentially all the other processing tasks such as noise removal, image edge detection, distortion restoration, feature extraction, enhancement, segmentation, and pattern recognition. Although there are many mode-decomposition approaches, such as empirical mode decomposition (EMD),³¹ iterative filtering decomposition^{41,70} and wavelets, partial differential equation (PDE) approaches have not been discovered. A major obstacle is due to the limited understanding of high order PDEs. High order PDEs have been conventionally considered as unnecessary in physical modeling and computationally unstable. The present work constructs a PDE based framework for mode decomposition of signals, images and functions. We show that it takes an in-depth understanding of the performance and function of arbitrarily high order PDE based low-pass filters⁷³ and nonlinear PDE based high-pass filters⁷⁶ to construct PDE based methods for mode decomposition analysis. Inspired by our mode decomposition via iterative filtering,^{41,70} we propose a family of mode decomposition evolution equations (MoDEEs) in the present paper. The construction of MoDEEs is equivalent to the design of high order PDE based high-pass filters. The proposed MoDEEs yield band-frequency components (or modes) by recursively extracting high frequency signals using high order PDEs. MoDEEs behave like Fourier transform and wavelet transform — the intrinsic modes generated from MoDEEs have a perfect reconstruction of the original function. In this sense, we also call the operation of MoDEEs a PDE transform. However, the proposed PDE transform is capable of decomposing signals and images into various “functional” modes instead of pure frequency modes like those in Fourier transform. By functional modes, we mean the components which share similar band of frequencies or belong to same category, e.g., noise, edge and trend. But unlike wavelet transform, the proposed PDE transform works like a series of low-pass and/or high-pass filters in the spatial or time domain only. As such, the subsequent secondary processing on each individual mode becomes robust and controllable, leading to desirable processing effects. The Fourier pseudospectral method has been utilized in our numerical solution of high order PDEs. This method is unconditionally stable and very efficient for linearized MoDEEs.

The present MoDEE approach is carefully validated on several benchmark testing cases to demonstrate its ability, usefulness, and efficiency. We first consider the standard test of mode separating of signals and functions. We have shown that the proposed MoDEEs are able to effectively split high frequency adjacent modes. Such a result enable us to separate noise from signals in many situation and perform many other secondary processing tasks. The applications of the present MoDEEs are considered to image edge detection, feature extraction, denoising and enhancement. We purposely choose to apply the method to various types of medical images obtained using MRI, MRA or CT.

The proposed MoDEEs can be extended a number of ways. First, different forms of MoDEEs can be constructed based on the proposed principles. This can be formulated as a problem of variation for a given application. Additionally, the role of nonlinear PDEs will be explored. Anisotropic diffusion type of schemes are expected to yield better results. Moreover, computational methods for nonlinear high order MoDEEs deserve a further study. Stable scheme is crucial for the implementation of high order PDEs. Furthermore, parameter optimization is an important issue in the MoDEE applications too. Finally, more general applications, such as to regression analysis, linear programming and machine learning are possible. These aspects are under our consideration.

Acknowledgments

This work was supported in part by NSF grants CCF-0936830 and DMS-1043034; NIH grant GM-090208; MSU Competitive Discretionary Funding Program grant 91-4600.

Literature cited

- [1] S. Angenent, E. Pichon, and A. Tannenbaum. Mathematical methods in medical image processing. *Bulletin of the American Mathematical Society*, 43(3):365–396, 2006.
- [2] R. Archibald, A. Gelb, R. Saxena, and D. B. Xiu. Discontinuity detection in multivariate space for stochastic simulations. *Journal of Computational Physics*, 228(7):2676–2689, 2009.
- [3] R. Archibald, A. Gelb, and J. H. Yoon. Polynomial fitting for edge detection in irregularly sampled signals and images. *SIAM Journal on Numerical Analysis*, 43(1):259–279, 2005.
- [4] T. Barbu, V. Barbu, V. Biga, and D. Coca. A PDE variational approach to image denoising and restoration. *Nonlinear Analysis Real World Applications*, 10(3):1351–1361, 2009.
- [5] P. W. Bates, Z. Chen, Y. H. Sun, G. W. Wei, and S. Zhao. Geometric and potential driving formation and evolution of biomolecular surfaces. *Journal of Mathematical Biology*, 59(2):193–231, 2009.
- [6] M. Bertalmio. Strong-continuation, contrast-invariant inpainting with a third-order optimal PDE. *IEEE Transactions on Image Processing*, 15(7):1934–1938, 2006.
- [7] A. L. Bertozzi and J. B. Greer. Low-curvature image simplifiers: Global regularity of smooth solutions and laplacian limiting schemes. *Communications on Pure and Applied Mathematics*, 57(6):764–790, 2004.
- [8] R. B. Buxton. *Introduction to functional magnetic resonance imaging – principles and techniques*. Cambridge University Press, Cambridge, UK, 2002.
- [9] J. Canny. A computational approach to edge-detection. *IEEE Transactions on Pattern Analysis and Machine Intelligence*, 8(6):679–698, 1986.
- [10] V. Caselles, J. M. Morel, G. Sapiro, and A. Tannenbaum. Introduction to the special issue on partial differential equations and geometry-driven diffusion in image processing and analysis. *IEEE Transactions on Image Processing*, 7(3):269–273, 1998.
- [11] F. Catte, P. L. Lions, J. M. Morel, and T. Coll. Image selective smoothing and edge-detection by nonlinear diffusion. *SIAM Journal on Numerical Analysis*, 29(1):182–193, 1992.
- [12] A. Chambolle and P. L. Lions. Image recovery via total variation minimization and related problems. *Numerische Mathematik*, 76(2):167–188, 1997.
- [13] T. Chan, A. Marquina, and P. Mulet. High-order total variation-based image restoration. *SIAM Journal on Scientific Computing*, 22(2):503–516, 2000.
- [14] T. Chan and J. Shen. *Image processing and analysis: variational, PDE, wavelet, and stochastic methods*. Society for Industrial Mathematics, 2005.
- [15] Y. Chan. *Wavelet basics*. Springer, 1995.
- [16] K. Chen, X. Chen, R. Renaut, G. E. Alexander, D. Bandy, H. Guo, and E. M. Reiman. Characterization of the image-derived carotid artery input function using independent component analysis for the quantitation of 18f fluorodeoxyglucose positron emission tomography images. *Physics in Medicine and Biology*, 52(23):7055–7071, 2007.
- [17] Q. H. Chen, N. Huang, S. Riemenschneider, and Y. S. Xu. A B-spline approach for empirical mode decompositions. *Advances in Computational Mathematics*, 24(1-4):171–195, 2006.
- [18] Z. Chen, N. A. Baker, and G. W. Wei. Differential geometry based solvation models I: Eulerian formulation. *J. Comput. Phys. (accepted)*, 2010.

- [19] I. Daubechies. *Ten Lectures on Wavelets*. SIAM, Philadelphia, 1992.
- [20] J. C. Echeverria, J. A. Crowe, M. S. Woolfson, and B. R. Hayes-Gill. Application of empirical mode decomposition to heart rate variability analysis. *Medical and Biological Engineering and Computing*, 39(4):471–479, 2001.
- [21] M. Farge. Wavelet transforms and their applications to turbulence. *Annual Review of Fluid Mechanics*, 24:395–457, 1992.
- [22] G. Gilboa, N. Sochen, and Y. Y. Zeevi. Forward-and-backward diffusion processes for adaptive image enhancement and denoising. *IEEE Transactions on Image Processing*, 11(7):689–703, 2002.
- [23] G. Gilboa, N. Sochen, and Y. Y. Zeevi. Image sharpening by flows based on triple well potentials. *Journal of Mathematical Imaging and Vision*, 20(1-2):121–131, 2004.
- [24] J. B. Greer and A. L. Bertozzi. H-1 solutions of a class of fourth order nonlinear equations for image processing. *Discrete and Continuous Dynamical Systems*, 10(1-2):349–366, 2004.
- [25] J. B. Greer and A. L. Bertozzi. Traveling wave solutions of fourth order PDEs for image processing. *SIAM Journal on Mathematical Analysis*, 36(1):38–68, 2004.
- [26] V. Grimm, S. Henn, and K. Witsch. A higher-order PDE-based image registration approach. *Numerical Linear Algebra with Applications*, 13(5):399–417, 2006.
- [27] Y. Gu and G. W. Wei. Conjugate filter approach for shock capturing. *Communications in Numerical Methods in Engineering*, 19(2):99–110, 2003.
- [28] H. Guo, R. Renaut, and K. Chen. An input function estimation method for FDG-PET human brain studies. *Nuclear medicine and biology*, 34(5):483–492, 2007.
- [29] H. Guo, R. A. Renaut, K. Chen, and E. Reiman. FDG-PET parametric imaging by total variation minimization. *Computerized Medical Imaging and Graphics*, 33(4):295–303, 2009.
- [30] E. M. Haacke, R. W. Brown, M. R. Thompson, and R. Venkatesan. *Magnetic resonance imaging: physical principles and sequence design*. Wiley, New York, 1999.
- [31] N. E. Huang, S. R. Long, and Z. Shen. The mechanism for frequency downshift in nonlinear wave evolution. *Advances in Applied Mechanics, Vol 32*, 32:59, 1996.
- [32] N. E. Huang, Z. Shen, and S. R. Long. A new view of nonlinear water waves: The Hilbert spectrum. *Annual Review of Fluid Mechanics*, 31:417–457, 1999.
- [33] N. E. Huang, Z. Shen, S. R. Long, M. L. C. Wu, H. H. Shih, Q. N. Zheng, N. C. Yen, C. C. Tung, and H. H. Liu. The empirical mode decomposition and the Hilbert spectrum for nonlinear and non-stationary time series analysis. *Proceedings of the Royal Society of London Series a-Mathematical Physical and Engineering Sciences*, 454(1971):903–995, 1998.
- [34] A. K. Jain. Partial-differential equations and finite-difference methods in image-processing .1. image representation. *Journal of Optimization Theory and Applications*, 23(1):65–91, 1977.
- [35] J. H. Jin and J. J. Shi. Feature-preserving data compression of stamping tonnage information using wavelets. *Technometrics*, 41(4):327–339, 1999.
- [36] Z. M. Jin and X. P. Yang. Strong solutions for the generalized Perona-Malik equation for image restoration. *Nonlinear Analysis-Theory Methods and Applications*, 73(4):1077–1084, 2010.
- [37] D. A. Karras and G. B. Mertzios. New PDE-based methods for image enhancement using SOM and bayesian inference in various discretization schemes. *Measurement Science Technology*, 20(10):8, 2009.

- [38] Y. Kopsinis and S. McLaughlin. Development of EMD-based denoising methods inspired by wavelet thresholding. *IEEE Transactions on Signal Processing*, 57(4):1351–1362, 2009.
- [39] S. Li. *Markov random field modeling in image analysis*. Springer-Verlag New York Inc, 2009.
- [40] H. L. Liang, Q. H. Lin, and J. D. Z. Chen. Application of the empirical mode decomposition to the analysis of esophageal manometric data in gastroesophageal reflux disease. *IEEE Transactions on Biomedical Engineering*, 52(10):1692–1701, 2005.
- [41] L. Lin, Y. Wang, and H. Zhou. Iterative filtering as an alternative algorithm for empirical mode decomposition. *Advances in Adaptive Data Analysis*, 1(4):543–560, 2009.
- [42] B. Liu, S. Riemenschneider, and Y. Xu. Gearbox fault diagnosis using empirical mode decomposition and Hilbert spectrum. *Mechanical Systems and Signal Processing*, 20(3):718–734, 2006.
- [43] M. Lysaker, A. Lundervold, and X. C. Tai. Noise removal using fourth-order partial differential equation with application to medical magnetic resonance images in space and time. *IEEE Transactions on Image Processing*, 12(12):1579–1590, 2003.
- [44] S. Mallat. *A Wavelet tour of signal processing*. Academic Press, 1999.
- [45] D. Mao, D. Rockmore, Y. Wang, and Q. Wu. EMD Analysis for Visual Stylogmetry. *Preprint*.
- [46] D. Mao, D. N. Rockmore, Y. Wang, and Q. Wu. Emd analysis for visual stylometry. *Preprint*.
- [47] D. Mao, Y. Wang, and Q. Wu. A New Approach for Analyzing Physiological Time Series. *Preprint*.
- [48] D. Mao, Y. Wang, and Q. Wu. A new approach for analyzing physiological time series. *Preprint*.
- [49] D. Marr and E. Hildreth. Theory of edge-detection. *Proceedings of the Royal Society of London Series B-Biological Sciences*, 207(1167):187–217, 1980.
- [50] F. G. Meyer and R. R. Coifman. Brushlets: A tool for directional image analysis and image compression. *Applied and Computational Harmonic Analysis*, 4(2):147–187, 1997.
- [51] M. Nitzberg and T. Shiota. Nonlinear image filtering with edge and corner enhancement. *IEEE Transactions on Pattern Analysis and Machine Intelligence*, 14(8):826–833, 1992.
- [52] A. V. Oppenheim and R. W. Schaffer. *Digital Signal Process*. Englewood Cliffs, NJ: Prentice-Hall, 1989.
- [53] P. Perona and J. Malik. Scale-space and edge-detection using anisotropic diffusion. *IEEE Transactions on Pattern Analysis and Machine Intelligence*, 12(7):629–639, 1990.
- [54] M. Pesenson, W. Roby, and B. McCollum. Multiscale astronomical image processing based on nonlinear partial differential equations. *Astrophysical Journal*, 683(1):566–576, 2008.
- [55] R. J. Radke, S. Andra, O. Al-Kofahi, and B. Roysam. Image change detection algorithms: A systematic survey. *IEEE Transactions on Image Processing*, 14(3):294–307, 2005.
- [56] D. Rezaei and F. Taheri. Experimental validation of a novel structural damage detection method based on empirical mode decomposition. *Smart Materials and Structures*, 18(4), 2009.
- [57] G. Rilling, P. Flandrin, P. Goncalves, and J. M. Lilly. Bivariate empirical mode decomposition. *IEEE Signal Processing Letters*, 14:936–939, 2007.
- [58] L. I. Rudin, S. Osher, and E. Fatemi. Nonlinear total variation based noise removal algorithms. *Physica D*, 60(1-4):259–268, 1992.

- [59] R. Saxena, A. Gelb, and H. Mittelman. A high order method for determining the edges in the gradient of a function. *Communications in Computational Physics*, 5(2-4):694–711, 2009.
- [60] Y. Shih, C. Rei, and H. Wang. A novel PDE based image restoration: Convection-diffusion equation for image denoising. *Journal of Computational and Applied Mathematics*, 231(2):771–779, 2009.
- [61] K. Siddiqi, B. B. Kimia, and C. W. Shu. Geometric shock-capturing eno schemes for subpixel interpolation, computation and curve evolution. *Graphical Models and Image Processing*, 59(5):278–301, 1997.
- [62] G. R. Spedding, F. K. Browand, N. E. Huang, and S. R. Long. A 2-d complex wavelet analysis of an unsteady wind-generated surface-wave field. *Dynamics of Atmospheres and Oceans*, 20(1-2):55–77, 1993.
- [63] G. R. Spedding, F. K. Browand, N. E. Huang, and S. R. Long. A 2-d complex wavelet analysis of an unsteady wind-generated surface-wave field. *Dynamics of Atmospheres and Oceans*, 20(1-2):55–77, 1993.
- [64] Y. H. Sun, P. R. Wu, G. Wei, and G. Wang. Evolution-Operator-Based Single-Step Method for Image Processing. *Int. J. Biomed. Imaging*, 83847:1, 2006.
- [65] Y. H. Sun, Y. C. Zhou, S. G. Li, and G. W. Wei. A windowed Fourier pseudospectral method for hyperbolic conservation laws. *Journal of Computational Physics*, 214(2):466–490, 2006.
- [66] T. Tanaka and D. P. Mandic. Complex empirical mode decomposition. *IEEE Signal Processing Letters*, 14(2):101–104, 2007.
- [67] Y.-W. Tang, C.-C. Tai, C.-C. Su, C.-Y. Chen, and J.-F. Chen. A correlated empirical mode decomposition method for partial discharge signal denoising. *Measure. Science Tech.*, 21:085106, 2010.
- [68] T. Tasdizen, R. Whitaker, P. Burchard, and S. Osher. Geometric surface processing via normal maps. *Acm Transactions on Graphics*, 22(4):1012–1033, 2003.
- [69] E. C. Titchmarsh. *Introduction to the theory of Fourier integrals*. Oxford University Press, 1948.
- [70] Y. Wang, G. Wei, and S.-Y. Yang. Iterative filtering decomposition based on local spectral evolution kernel. *submitted*, 2010.
- [71] Y. Wang, Y. B. Zhao, and G. W. Wei. A note on the numerical solution of high-order differential equations. *Journal of Computational and Applied Mathematics*, 159(2):387–398, 2003.
- [72] Z. Wang, B. C. Vemuri, Y. Chen, and T. H. Mareci. A constrained variational principle for direct estimation and smoothing of the diffusion tensor field from complex DWI. *IEEE Trans. Medical Imaging*, 23:930, 2004.
- [73] G. W. Wei. Generalized Perona-Malik equation for image restoration. *IEEE Signal Processing Letters*, 6(7):165–167, 1999.
- [74] G. W. Wei. A unified approach for the solution of the Fokker-Planck equation. *Journal of Physics A: Mathematical and General*, 33:4935, 2000.
- [75] G. W. Wei. Oscillation reduction by anisotropic diffusions. *Comput. Phys. Commun.*, 144:417–342, 2002.
- [76] G. W. Wei and Y. Q. Jia. Synchronization-based image edge detection. *Europhysics Letters*, 59(6):814–819, 2002.

- [77] C.-F. Westin, S. E. Maier, H. Mamata, A. Nabavi, F. A. Jolesz, and R. Kikinis. Processing and visualization of diffusion tensor MRI. *Medical Image Analysis*, 6:93, 2002.
- [78] T. P. Witelski and M. Bowen. Adi schemes for higher-order nonlinear diffusion equations. *Applied Numerical Mathematics*, 45(2-3):331–351, 2003.
- [79] A. Witkin. Scale-space filtering: A new approach to multi-scale description. In *Proceedings of IEEE International Conference on Acoustic Speech Signal Processing*, volume 9, pages 150–153. Institute of Electrical and Electronics Engineers, 1984.
- [80] J. Y. Wu, Q. Q. Ruan, and G. Y. An. Exemplar-based image completion model employing PDE corrections. *Informatica*, 21(2):259–276, 2010.
- [81] M. Xu and S. L. Zhou. Existence and uniqueness of weak solutions for a fourth-order nonlinear parabolic equation. *Journal of Mathematical Analysis and Applications*, 325(1):636–654, 2007.
- [82] S.-Y. Yang, Y. C. Zhou, and G. W. Wei. Comparison of the discrete singular convolution algorithm and the Fourier pseudospectral method for solving partial differential equations. *Computer Physics Communications*, 143(2):113–135, 2002.
- [83] Y. You and M. Kaveh. Fourth-order partial differential equations for noise removal. *IEEE Transactions on Image Processing*, 9(10):1723–1730, 2002.
- [84] S. N. Yu, S. Zhao, and G. W. Wei. Local spectral time splitting method for first- and second-order partial differential equations. *Journal of Computational Physics*, 206(2):727–780, 2005.
- [85] S. Zhao and G. W. Wei. Comparison of the discrete singular convolution and three other numerical schemes for solving fisher’s equation. *SIAM Journal on Scientific Computing*, 25(1):127–147, 2003.
- [86] S. Zhao and G. W. Wei. Matched interface and boundary (MIB) for the implementation of boundary conditions in high-order central finite differences. *International Journal for Numerical Methods in Engineering*, 77(12):1690–1730, 2009.